Lab on a Chip

RSCPublishing

"Microfluidic drifting"—implementing three-dimensional hydrodynamic focusing with a single-layer planar microfluidic device†

Xiaole Mao,[ab] John Robert Waldeisen[a] and Tony Jun Huang*[ab]

We introduce a novel fluid manipulation technique named "microfluidic drifting" to enable three-dimensional (3D) hydrodynamic focusing with a simple single-layer planar microfluidic device.

Hydrodynamic focusing is one of the most utilized techniques in microfluidics. Its applications have been employed in a wide variety of chemical/biological analyses, including on-chip flow cytometry,[1,2] single molecule detection,[3] and laminar mixers for the study of rapid chemical and enzymatic kinetics.[4–6] The principle of hydrodynamic focusing is simple: a central sample solution with a low flow rate flows within an outer fluid sheath traveling at a higher flow rate, thus enabling the compression of the inner sample flow. However, the planar nature of the two-dimensional (2D) microfluidic network fabricated via standard soft lithography only facilitates the 2D hydrodynamic focusing in the device plane by horizontally compressing the inner sample flow into a thin "sheet" between two sheath flows injected from both sides of the sample flow. Consequently, there arises an inability to focus the sample flow in the vertical (out-of-plane) direction.

In many cases, 2D hydrodynamic focusing is intrinsically problematic due to the lack of vertical focusing. The non-uniform velocity distribution of vertically spread cells or molecules is known to cause complications in flow cytometry.[2,7] For on-chip single molecule detection, which requires passage of the sample through a minute optical detection region much smaller than the size of the channel, the vertical spread of sample results in a large number of undetected molecules.[8] In the laminar mixer, flow velocity variations of the focused enzymes or chemical species in the vertical direction[5] may result in a different reaction time across the depth of the channel, which would make it extremely difficult to extract meaningful information of reaction kinetics. These problems could be solved by using an axis-symmetric focusing device, which consists of two concentric capillaries.[6,9] However, in practice, such structures are hard to fabricate using the photolithography based microfabrication technique. As a result, the massive production of such devices would be difficult. Therefore, there has been a great interest in developing microfabricated devices that are capable of focusing the sample stream in both horizontal and vertical directions. Such a focusing method adds an additional dimension of control over the sample flow as compared to the traditional 2D focusing, and therefore it is often referred to as three-dimensional (3D) hydrodynamic focusing.

Until now, only a few microfabricated 3D hydrodynamic focusing devices have been reported.[2,10–13] In these studies, 3D focusing is achieved by delivering sheath flows from both vertical and horizontal directions using multi-layer 3D microfluidic devices. Multi-step photolithography and assembly protocols have been developed for fabricating the 3D microfluidic structures needed for 3D hydrodynamic focusing. However, such methods require either tedious assembly of individual components or multiple alignments and exposures during mold fabrication. These limitations inevitably increase the cost and complexity of the device and ultimately hinder their applicability.

In this work, we demonstrate how state-of-the-art fluid manipulation enables 3D hydrodynamic focusing with a simple single-layer planar microfluidic device fabricated via standard soft lithography. The mechanism of 3D focusing is illustrated in Fig. 1 using a computational fluid dynamic (CFD) simulation (CFD-ACE+, ESI-CFD). The device shown here includes four inlets for sample and sheath flows, one outlet, and a 90-degree curve with a mean radius of 250 μm. The widths of channels for the sample
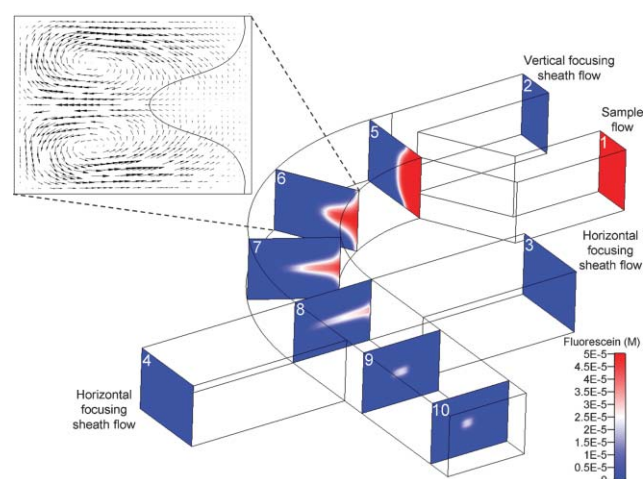
[a]Department of Engineering Science and Mechanics, The Pennsylvania State University, University Park, PA 16802, USA.
E-mail: junhuang@psu.edu; Fax: +1-814-865-9974;
Tel: +1-814-863-4209
[b]Department of Bioengineering, The Pennsylvania State University, University Park, PA 16802, USA
† Electronic supplementary information (ESI) available: Real-time video of Fig. 2c and Fig. 2d and details of CFD simulation and device fabrication. See DOI: 10.1039/b711155j

Fig. 1 Schematic of the 3D hydrodynamic focusing process by employing the "microfluidic drifting" technique. Slices 1–10 are the cross-sectional profiles of the fluorescein dye concentration in the focusing device. Inset: the simulation of the secondary flow velocity field shows the formation of Dean vortices in the 90-degree curve. An iso-curve of fluorescein concentration = 25 μM is arbitrarily chosen as the boundary of the sample flow.

flow and the vertical focusing sheath flow are 50 µm and the two side channels for horizontal focusing sheath flows are 100 µm wide. The width of the main channel is 100 µm and the channel depth throughout the entire device is 75 µm. The 3D hydrodynamic focusing is accomplished in a two-step sequence. The first step focuses the sample flow in the vertical direction by using what we call the "microfluidic drifting" technique. This term refers to the lateral drift of the sample flow, caused by the transverse secondary flow induced by the centrifugal effect in the curve of a microfluidic channel.[14–18] The secondary flow is characterized by a pair of counter-rotating vortices (Dean vortices) positioned in the upper and lower portion of the channel cross-sectional plane. In Fig. 1, the sample flow (50 µM fluorescein dye solution, slice 1), and the vertical focusing sheath flow (water, slice 2) are co-infused into the 90-degree curve at flow rates of 50 µl min^{-1} and 337 µl min^{-1}, respectively. Our calculation shows in the main channel the Reynolds number $Re \approx 74$ ($Re = \rho V D/\mu$, where ρ is fluid density, V is the average flow velocity, D is the hydraulic diameter of channel, and μ is the fluid viscosity) and the Dean number $\kappa \approx 43$ ($\kappa = \delta^{0.5}Re$, $\delta = D/R$, where R is mean radius of the curve). Under this flow condition, a strong secondary Dean effect is expected in theory.[16–18] This is confirmed by the Dean vortices found in the simulation of the induced secondary flow velocity field (Fig. 1 inset). The induced Dean vortices act to transversely transport the fluid, causing the sample flow to drift laterally to the opposite side of channel (slices 5–8). The final cross-sectional profile of the drifted sample flow at the exit of the curve (slice 8) is flow rate dependent: the combined flow rate of the vertical focusing sheath flow and sample flow determines the extent of lateral drift, and the flow rate ratio between the vertical focusing sheath flow and the sample flow controls the compression ratio in the vertical direction. Flow rates are carefully selected based on factors, such as fluid properties[15] and device geometries (*i.e.*, the aspect ratio and radius of the curve)[16–18] so that the sample flow can be "stretched" into a thin horizontal flow and vertically focused between the split vertical focusing sheath flows (slice 8). Focusing in the horizontal direction (slices 8–10) is conducted with two horizontal focusing sheath flows (water, slices 3 and 4) at the flow rates of 225 µl min^{-1}, which further compress the vertically focused sample flow from both sides. The combined effects of these two focusing steps result in a 3D hydrodynamically focused sample flow in the center of the microfluidic channel. The cross-sectional dimensions of the focused flow in both vertical and

horizontal directions and its horizontal position can be individually tuned: flow rates of vertical focusing sheath flow and the sample flow control the height in the vertical direction; the ratio between the rate of horizontal focusing sheath flow and the total rate of the vertical focusing sheath flow and sample flow determines the width; and the horizontal position of the final 3D focused flow can be shifted by changing the ratio of the two horizontal focusing sheath flows.

The device design and optical setup for creating and characterizing the 3D focused flow is shown in Fig. 2. Briefly, the microfluidic channel is made by casting the PDMS on a planar silicon mold fabricated using the standard photolithography and deep reactive ion etching (DRIE).† To observe the focusing in the vertical direction, a smooth, transparent optical window is placed adjacent to the main channel to allow the "side-view imaging" of the focused flow. The PDMS substrate was cut along the "PDMS cut line" to expose the optical window to a light source (Fig. 2a). A 45-degree prism is placed adjacent to the optical window to deflect the excitation light and emission light so the side-view profile of the focused flow can be monitored using an epifluorescence microscope (Fig. 2b).

Experimentation of 3D hydrodynamic focusing was conducted as determined by the prior CFD simulations and visual evidence of 3D hydrodynamic focusing (both top-view and side-view) were obtained *via* epifluorescence microscopy. The fluorescein (50 µM) dyed sample flow and vertical focusing sheath flow (DI water) were co-infused into the 90-degree curve, and the horizontal focusing sheath flows (DI water) were injected from both sides. Fig. 3a depicts the top view of the fluorescent sample flow during the focusing process. Once entering the 90-degree curve, the sample flow starts to drift to the opposite side of the channel, visually evident by the increase in the width of the sample flow. The width of the sample flow reaches its maximum at the exit of the 90-degree curve, upon which the flow is compressed by the horizontal focusing sheath flows. A CFD simulation performed under the corresponding experimental conditions is shown in Fig. 3b and accurately replicates experimental observations. Fig. 3c depicts the side-view of the 3D focused flow in the main channel. The sample flow is found to be focused in the center of the channel, with a total height of less than 15 µm. Fig. 3d shows the side-view of the main channel after flows have been stopped. The fluorescent dye diffuses through the entire channel, resulting in a uniform distribution of fluorescent dye at a much lower concentration. It
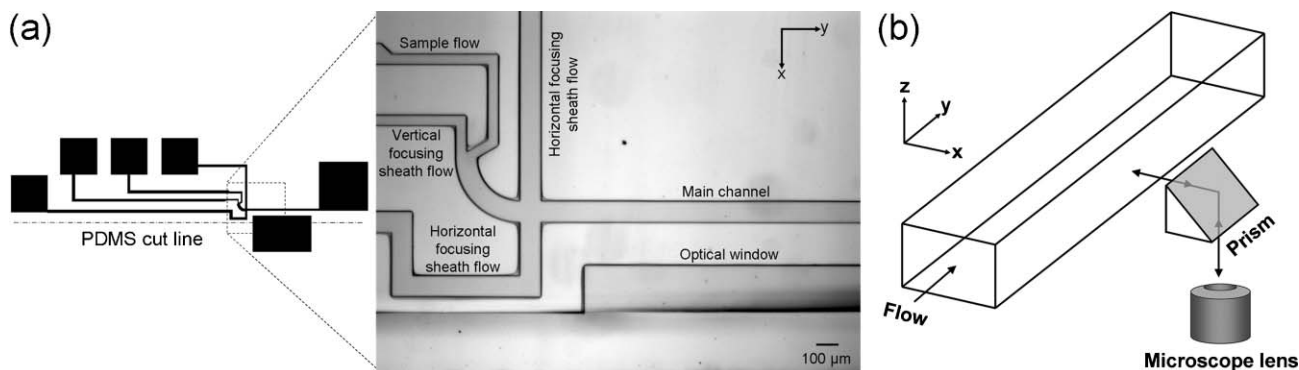

Fig. 2 (a) The photomask (left) and image (right) of the microfluidic device for creating and characterizing the 3D focused flow. (b) The schematic of the optical setup for the side-view epifluorescence imaging of the focused flow.
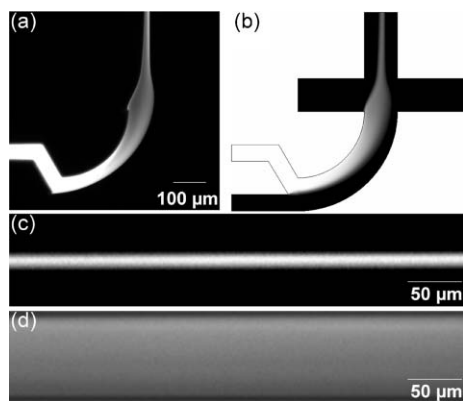
Fig. 3 (a) Top view of the sample flow pattern during the 3D focusing process and (b) CFD simulation under the same flow conditions. (c) Side-view of the 3D focused sample flow (flow direction: right to left) in the main channel and (d) the same view of the channel after the flow is stopped.
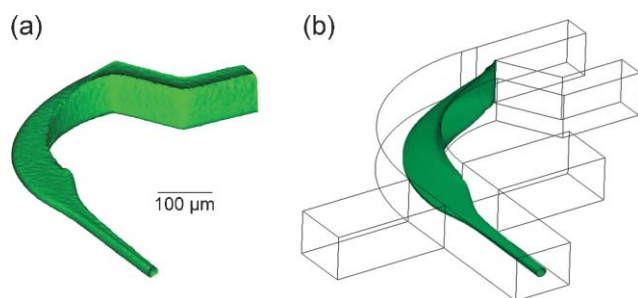

Fig. 4 (a) The 3D architecture of the sample flow during the focusing process characterized by confocal microscopy and (b) the CFD simulation performed under the same flow conditions (an iso-surface of fluorescein concentration = 15 μM is arbitrarily chosen as the boundary of the sample flow).

is also observed that switching between static flow and 3D focusing takes less than 3 s and is highly repeatable (illustrated in a real-time video in the ESI).†

Finally, confocal microscopy was conducted in order to reveal the full 3D architecture of the sample flow in the 3D hydrodynamic focusing process. The 3D structure of the sample flow is constructed using a Z-stacked series of fluorescent images scanned at 2 μm intervals. Fig. 4a depicts the 3D image of the sample flow and clearly reveals the microfluidic drifting in the curve, as well as the final 3D focused flow. Fig. 4b is a CFD simulation obtained with the same flow conditions. Strong agreement is evident between the confocal microscopic image and the simulated result.

In conclusion, this study has introduced a novel fluid manipulation technique named "microfluidic drifting", to allow 3D hydrodynamic focusing with a simple single-layer planar microfluidic device. This method is effective, robust, and most of all, does not require any extensive fabrication technique other than standard soft lithography. We believe microfluidic drifting may permit many applications that would otherwise not be possible, due to the current limitations of impractical and specialized 3D microfabrication techniques required for 3D hydrodynamic focusing.

Notes and references

1 M. M. Wang, E. Tu, D. E. Raymond, J. M. Yang, H. Zhang, N. Hagen, B. Dees, E. M. Mercer, A. H. Forster, I. Kariv, P. J. Marchand and W. F. Butler, *Nat. Biotechnol.*, 2005, **23**, 83–87.
2 A. Wolff, I. R. Perch-Nielsen, U. D. Larsen, P. Friis, G. Goranovic, C. R. Poulsen, J. P. Kutter and P. Telleman, *Lab Chip*, 2003, **3**, 22–27.
3 A. J. de Mello and J. B. Edel, *J. Appl. Phys.*, 2007, **101**, 084903.
4 J. B. Knight, A. Vishwanath, J. P. Brody and R. H. Austin, *Phys. Rev. Lett.*, 1998, **80**, 3863–3866.
5 L. Pollack, M. W. Tate, N. C. Darnton, J. B. Knight, S. M. Gruner, W. A. Eaton and R. H. Austin, *Proc. Natl. Acad. Sci. U. S. A.*, 1999, **96**, 10115–10117.
6 S. A. Pabit and S. J. Hagen, *Biophys. J.*, 2002, **83**, 2872–2878.
7 S. Eyal and S. R. Quake, *Electrophoresis*, 2002, **23**, 2653–2657.
8 T.-H. Wang, Y. Peng, C. Zhang, P. K. Wong and C.-M. Ho, *J. Am. Chem. Soc.*, 2005, **127**, 5354–5359.
9 S. Takeuchi, P. Garstecki, D. B. Weibel and G. M. Whitesides, *Adv. Mater.*, 2005, **17**, 1067–1072.
10 N. Sundararajan, M. S. Pio, L. P. Lee and A. A. Berlin, *J. Microelectromech. Syst.*, 2004, **13**, 559–567.
11 C. Simonnet and A. Groisman, *Appl. Phys. Lett.*, 2005, **87**, 114104.
12 R. Yang, D. L. Feeback and W. Wang, *Sens. Actuators, A*, 2005, **118**, 259–267.
13 C.-C. Chang, Z.-X. Huang and R.-J. Yang, *J. Micromech. Microeng.*, 2007, **17**, 1479–1486.
14 Y. Yamaguchi, F. Takagi, K. Yamashita, H. Nakamura, H. Maeda, K. Sotowa, K. Kusakabe, Y. Yamasaki and S. Morooka, *AIChE J.*, 2004, **50**, 1530–1535.
15 X. Mao, J. R. Waldeisen, B. K. Juluri and T. J. Huang, *Lab Chip*, 2007, DOI: 10.1039/b708863a.
16 P. B. Howell, Jr., D. R. Mott, J. P. Golden and F. S. Ligler, *Lab Chip*, 2004, **4**, 663–669.
17 A. P. Sudarsan and V. M. Ugaz, *Lab Chip*, 2006, **6**, 74–82.
18 A. P. Sudarsan and V. M. Ugaz, *Proc. Natl. Acad. Sci. U. S. A.*, 2006, **103**, 7228–7233.